Thin Solid Films 534 (2013) 198–204

Contents lists available at SciVerse ScienceDirect

Thin Solid Films

journal homepage: www.elsevier.com/locate/tsf

Properties of $SiAlO_2N$ protective coatings on surface acoustic wave devices

Blake T. Sturtevant [a,c,*], Mauricio Pereira da Cunha [b,c], Robert J. Lad [a,c]

[a] Department of Physics & Astronomy, University of Maine, Orono, ME 04469-5708, USA
[b] Department of Electrical & Computer Engineering, University of Maine, Orono, ME 04469-5708, USA
[c] Laboratory for Surface Science & Technology, University of Maine, Orono, ME 04469-5708, USA

ARTICLE INFO

Article history:
Received 12 June 2012
Received in revised form 21 February 2013
Accepted 22 February 2013
Available online 5 March 2013

Keywords:
Silicon aluminum oxynitride
Protective coatings
Elastic moduli
Surface acoustic wave devices

ABSTRACT

The use of a protective wear-resistant amorphous $SiAlO_2N$ thin film overlayer (amorphous SiO_2–AlN alloy) on top of surface acoustic wave (SAW) devices is demonstrated on both quartz and langatate substrates. $SiAlO_2N$ films were deposited by RF magnetron sputtering onto sapphire substrates, quartz SAW devices, and langatate SAW devices. The $SiAlO_2N$ layer had an amorphous structure, a density of 2.8 ± 0.1 g/cm^3, a roughness less than 1 nm as measured by X-ray reflectivity, and a dielectric permittivity of 7.5 ± 0.05 as determined from microfabricated $SiAlO_2N$ capacitors. $SiAlO_2N$ elastic constants C_{11} and C_{44} were extracted using a numerical implementation of the matrix method for SAWs traveling in multilayer structures, and were found to be $C_{11} = 160 \pm 30$ GPa and $C_{44} = 55 \pm 5$ GPa. The operating frequencies of quartz SAW devices covered with $SiAlO_2N$ coatings were only slightly perturbed, but the temperature coefficient of delay (TCD) near 100 °C increased significantly by 250 ppm/°C. For langatate SAW devices, the $SiAlO_2N$ coating contributed an additional 8.5 dB to device transmission loss but the TCDs were minimally affected for $SiAlO_2N$ thicknesses up to 800 nm. This result suggests that langatate SAW devices for which temperature-frequency characteristics are important can be designed without consideration of the multi-layer structure, which greatly simplifies device design and modeling.

1. Introduction

Piezoelectric single crystals such as gallium phosphate ($GaPO_4$) and the LGX family, including langasite ($La_3Ga_5SiO_{14}$), langatate ($La_3Ga_{5.5}Ta_{0.5}O_{14}$), and langanite ($La_3Ga_{5.5}Nb_{0.5}O_{14}$), have been recently studied as potential alternatives to quartz in RF communication and sensor acoustic wave device applications [1–4]. These materials exhibit higher piezoelectric coupling compared to quartz, have experimentally demonstrated temperature compensated orientations, and can operate at significantly higher temperatures than quartz, which is no longer piezoelectric above its crystalline phase transition at 573 °C [5]. Gallium phosphate retains its piezoelectricity up to 933 °C [1], while the LGX family remain piezoelectric up to their melting points at or above 1470 °C [1]. To use these materials as microwave acoustic sensor devices in high temperature and/or harsh environments, not only does the piezoelectric bulk crystal need to remain stable, but the crystal surface and device electrodes also need to resist mechanical and chemical degradation during operation. For example, to transmit power using surface acoustic waves (SAWs), the surface of the piezoelectric crystal must have a roughness much smaller than the SAW wavelength, typically a few microns or less. In this paper, we discuss the use of $Si_xAl_yO_zN_{1-x-y-z}$ thin film overlayer coatings (denoted as 'SiAlON') deposited on top of SAW devices as a way of achieving protection against surface scratching and pitting of the piezoelectric crystal as well as protecting the device electrodes against oxidation or chemical degradation.

SiAlON ceramics have desirable hardness, wearability, and fracture toughness properties that make them useful materials in a variety of high temperature applications including gas turbines, high speed cutting tools, ceramic valves and piston pins, and turbocharger rotors [6–9]. When deposited in thin film form by reactive RF magnetron sputtering, SiAlON coatings are amorphous, are extremely smooth, and exhibit excellent wear resistance [8]. These properties of SiAlON films, along with the ease of manufacture on top of fabricated SAW devices, make them excellent candidates as protective layers for acoustic devices deployed in harsh environments.

Previous reports have shown that thin film overlayers on top of SAW devices can be used to reduce wear in SAW-driven linear motors [10] or to provide an oxidation barrier for interdigital transducer (IDT) electrodes at high temperatures [11,12]. When thin film coatings are present on top of the SAW devices, parameters such as transmission loss, operating frequency, and temperature behavior can be significantly modified from the bare device values, particularly if the films are thick relative to the wavelength of the SAW device [13–18]. For example, SiO_2 films with a thickness of 6 μm ($h/\lambda \approx 60\%$ where h is the film thickness and λ is the SAW wavelength) have been used on top of lithium tantalate SAW devices to purposefully change the

* Corresponding author at: Los Alamos National Laboratory; Materials Physics and Applications; PO Box 1663, MS D429; Los Alamos, NM USA 87545. Tel.: +1 505 606 2243; fax: +1 505 665 4292.
E-mail address: bsturtev@lanl.gov (B.T. Sturtevant).

0040-6090/$ – see front matter
http://dx.doi.org/10.1016/j.tsf.2013.02.062

temperature coefficient of delay (TCD) [14]. $TCD = \frac{1}{\tau}\frac{d\tau}{dT}$, where τ is the SAW group delay between IDTs and T is the temperature, is an important measure of how thermally stable an acoustic wave device is. Accurate design and modeling of SAW devices require that the acoustic wave characteristics of thin film overlayer coatings be precisely known.

The most important physical properties that are needed for modeling of SAW devices covered with a thin film overlayer are the film density, thickness, dielectric permittivity, and elastic moduli [16,19]. Since the elastic moduli of SiAlON materials are known to depend on their specific stoichiometry [20], it is very important to deposit the films under precise control and fully characterize them in terms of composition, structure, and modulus, and to determine how the resulting film properties influence SAW device behavior. In this work, we have chosen a single film stoichiometry, $SiAlO_2N$, for all of the experiments, and have determined the film elastic moduli from group velocity measurements of surface acoustic waves traveling on the $SiAlO_2N$ covered substrates. The influence of $SiAlO_2N$ overlayers on SAW device operating frequency and temperature coefficient of delay has also been measured, thereby enabling optimum SAW device design and modeling for operation in harsh environments.

2. Experimental details

$SiAlO_2N$ thin films were deposited to nominal thicknesses of 20 nm, 200 nm, and 800 nm onto r-cut sapphire substrates, quartz SAW devices, and langatate (LGT) SAW devices in an ultra-high vacuum deposition chamber that is directly coupled to an analysis chamber for determination of film composition using X-ray photoelectron spectroscopy (XPS) [21]. Depositions were performed by reactive RF magnetron co-sputtering of aluminum and silicon targets in an $Ar/O_2/N_2$ atmosphere at a pressure of 0.4 ± 0.07 Pa. The magnetron sources were operated with an RF power of 110 W and 130 W for the Si and Al targets, respectively, and the deposition rate (0.55 Å/s) was monitored by a quartz crystal oscillator. The substrate temperature was not actively controlled and typically rose to ~40 °C over the course of the deposition.

The chemical composition of each $SiAlO_2N$ film was measured with XPS using a SPECs Phoibos-HSA 3000 hemispherical electron analyzer, operated with a 20 eV pass energy in fixed analyzer transmission mode. Areas of the Si2p, Al2p, O1s, and N1s photoelectron peaks were used to quantify the stoichiometry, using a Shirley background subtraction [22] and relative sensitivity factor corrections [23]. Twelve $SiAlO_2N$ films grown on sapphire substrates had the following mean elemental percent compositions: Si: 19 ± 1 at.%, Al: 20 ± 1 at.%, N: 20 ± 2 at.%, and O: 41 ± 2 at.%, where the uncertainties are given by the standard deviation of the film compositions. Films with this stoichiometry can also be thought of as SiO_2–AlN amorphous alloys. This same film composition was also used on all of the SAW devices.

X-ray diffraction (XRD) and X-ray reflectivity (XRR) were used to determine the structure, density, roughness, and thickness of a set of $SiAlO_2N$ films grown on bare r-cut $(10\bar{1}2)$ sapphire substrates. The XRD and XRR measurements were performed with a PANalytical X'Pert Pro MRD diffractometer using Cu Kα radiation. The XRD measurements used the Bragg–Brentano geometry with a 1/16° fixed divergence slit on the incident beam side and a 100 channel PANalytical X'Celerator detector with Soller slits on the diffracted beam side. For the XRR measurements, the experimental setup consisted of an X-ray mirror and 1/16° fixed divergence slit on the incident beam side and a 0.27° parallel plate collimator fitted with a receiving slit on the diffracted beam side. XRR scans were started at $\omega = 0.1°$, well below the critical angle of both the film and substrate, and were stopped when the reflected intensity fell below the noise floor, typically around $2° < \omega < 3°$.

Parallel plate capacitors with a $SiAlO_2N$ thin film dielectric layer were fabricated on fused quartz substrates to determine the $SiAlO_2N$ dielectric permittivity (Fig. 1a & b). A 200 nm thick Al ground plane was sputter deposited on top of the substrate, and a stainless steel mask was placed over one corner prior to the $SiAlO_2N$ deposition to allow for electrical contact with the ground plane. Following

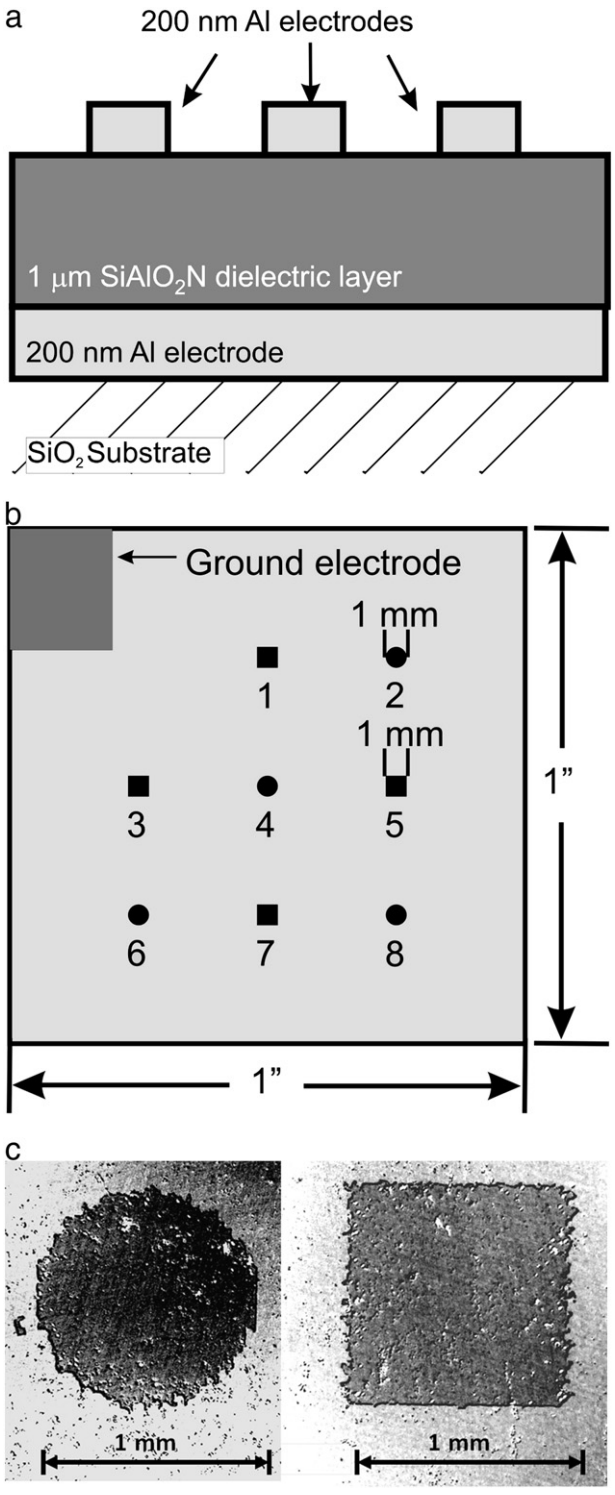

Fig. 1. $SiAlO_2N$ capacitors: (a) side view schematic showing layer thicknesses and (b) top view schematic showing layout of electrodes for measuring capacitance. During the $SiAlO_2N$ deposition, one corner was masked off to allow for electrical contact with the ground plane. (c) Micrograph of Al electrodes used for $SiAlO_2N$ ε_r determination. Of the eight capacitors fabricated, four had circular electrodes and four had square electrodes as shown in (b).

deposition of a 1 μm thick $SiAlO_2N$ layer, Al top electrodes were photolithographically patterned as either 1 mm diameter circles or squares with 1 mm side length (Fig. 1c). Capacitances were measured using a microprobe station and an Agilent 4284A Precision LCR meter at 10 kHz, a frequency selected since it did not introduce parasitic measurement artifacts resulting from the experimental setup.

ST-cut quartz was used to fabricate SAW devices for extraction of elastic constants because quartz wafers are readily available and the acoustic properties of this substrate are very well known [24]. SAW devices were fabricated along two different orientations: (i) ST-X with Euler angles (0°, 132.75°, 0°) and (ii) ST-40° with Euler angles (0°, 132.75°, 40°). These two quartz orientations were chosen because they are the two orientations in the ST plane exhibiting no power flow angle, which simplifies device design. For each of the two orientations, four sets of four SAW delay lines were fabricated; a representative set of four SAW delay lines is shown in Fig. 2. All transducers, fabricated using 150 nm Al on top of a 15 nm Cr adhesion layer, had 50λ wide apertures and were 80λ in length. Within each set, the eight split-finger IDTs ($\lambda = 32$ μm) were identical, and the only difference between the devices was the delay path length between IDTs. For each orientation, one set of four devices was left bare and the remaining three sets of four devices were coated with three different $SiAlO_2N$ thicknesses: 20 nm, 200 nm, and 800 nm.

The S-parameters for the quartz SAW delay lines were measured at room temperature using an Agilent 8753 ES network analyzer and a Cascade Microtech RF probe station. 1601 measurement points were recorded in a 4 MHz wide window centered on the maximum of $|S_{21}|$. Time gating was used to remove electromagnetic feed-through, residual SAW triple transit, and other spurious acoustic reflections. These data were used in the extraction of the elastic constants C_{11} and C_{44}. The devices with the shortest delay length (labeled 'a' in Fig. 2) were measured between 15 °C and 135 °C at 10 °C intervals using the RF probe station, network analyzer, and a Temptronic thermal chuck with 0.1 °C resolution.

A set of six langatate (LGT) SAW devices in the (90°, 23°, Ψ) plane with propagation directions $\Psi = 0°, 13°, 48°, 77°, 119°, 123°$ was also fabricated. This plane was selected due to its piezoelectric coupling, K^2, in the plane reaching a value of close to 0.7% in the vicinity of temperature compensated orientations [4]. One LGT wafer, containing the $\Psi = 0°, 48°, 123°$ devices, was coated with 500 nm of $SiAlO_2N$, while the other wafer, with the $\Psi = 13°, 77°, 119°$ devices, was coated with 800 nm of $SiAlO_2N$. The TCDs of LGT (90°, 23°, Ψ) SAW devices covered with a $SiAlO_2N$ overlayer were also measured over the same temperature range as the quartz devices. For temperature measurements on both the quartz and LGT devices, a resistance temperature detector mounted on a substrate of the same thickness as that of the devices was used to accurately record the temperature at the surface of the substrate. For the LGT devices, the surface temperature diverged from the thermal chuck temperature by as much as 5 °C at the higher temperatures.

3. Results and discussion

3.1. $SiAlO_2N$ film structure, density, and thickness

The Θ–2Θ XRD scans from the $SiAlO_2N$ films exhibited a broad ~15° wide peak centered at $2\Theta = 13°$, corresponding to short range order in the film on the length scale of ~7 Å. Grazing incidence XRD, performed to avoid the large substrate diffraction peaks, also revealed no diffraction peaks from the $SiAlO_2N$ films, indicating that they are amorphous, in agreement with [8]. A representative XRR spectrum (Fig. 3) shows periodic interference fringes that arise between X-rays scattered from the surface and the film/substrate interface. *X'Pert Reflectivity* software (PANalytical) was used to determine film thickness by measuring the periodicity of the fringes as described in [25]. Film densities were determined by measuring the critical angle, ω_c where the XRR intensity falls to half of its maximum value. The measured density of all the $SiAlO_2N$ films was found to be 2.8 ± 0.1 g/cm^3, lower than the 3.7–4.1 g/cm^3 values reported for bulk SiAlON samples [20].

Using the determined film thicknesses and densities, simulated XRR spectra were created by the *X'Pert Reflectivity* software (Fig. 3). The accuracies in the extracted film thickness and density were evaluated by visual comparison of XRR simulated spectra with measured data. The precision of the film thickness measurements was better than 5 Å. Slight changes in the values of the film thickness and density lead to differences between simulated and experimental data which are readily detectable by visual inspection. For example, a change in the film thickness from 535 Å to 545 Å input into the simulation program leads to a change in the number of fringes present in the simulated spectrum from 33 to 34 between the angles of $0.3 < \omega < 2.9$. Compared to thickness changes, modifications to the film density had a less pronounced effect; the precision of the density determination was only ± 0.1 g/cm^3. The simulations were also used to extract film roughness. The angle at which an XRR spectrum begins

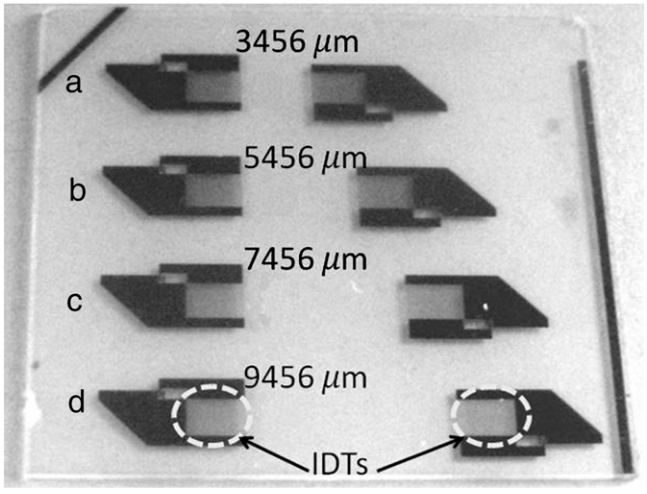

Fig. 2. SAW delay lines on quartz used for $SiAlO_2N$ elastic constant extraction. The IDTs of all devices are identical; the only difference between the devices is the length of the IDT center-to-center delay paths as indicated in the figure.

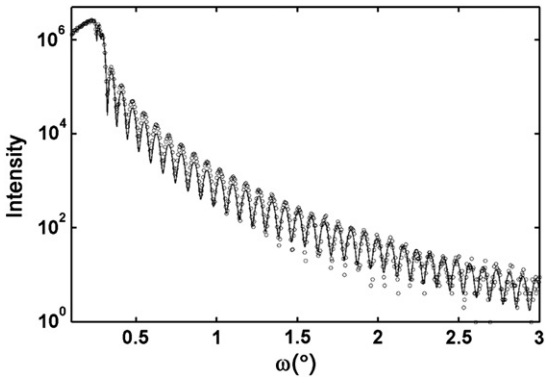

Fig. 3. An example of an X-ray reflectivity spectrum from a $SiAlO_2N$ thin film. A thickness of 535.0 Å was determined from the spacing of the fringes. The film density was determined to be 2.76 g/cm^3 from the location of the critical angle (the angle at which the intensity drops to half of its maximum value). The roughness of both the film surface and the interfacial boundaries was determined to be <10 Å from modeling the decay of the interference fringes. The circles denote measured data points and the solid trace corresponds to the modeled data.

to approach the noise level is inversely related to film roughness. For all $SiAlO_2N$ films studied, the roughness was determined to be 10 Å or less over the several mm^2 area probed by the X-ray beam, consistent with the fact that the XRR interference fringes persist to angles of $\omega \geq 3°$.

3.2. $SiAlO_2N$ film dielectric permittivity

The area of the electrodes in the capacitor structures used to measure dielectric permittivity was determined with an optical microscope at 50× magnification to an accuracy of better than 1 μm as validated by a Geller MicroÅnalytical MRS-3 magnification calibration standard. The uncertainty of the edge and radii length for these capacitors was ±15 μm corresponding to a 0.5% uncertainty in the relative dielectric constant. To verify the 1 μm thickness of the $SiAlO_2N$ layer, a mechanical profilometer was used since the upper limit for thickness determinations using XRR is around 400 nm. The actual thickness of the $SiAlO_2N$ layer was determined by the profilometer to be 998 ± 2 nm.

The measured capacitances, electrode areas, and extracted relative dielectric constants from the capacitors are shown in Table 1, where the capacitor numbers refer to the labels in Fig. 1b. The extracted permittivities, ε_r, were calculated using the well-known expression for an infinite parallel plate capacitor [26]: $C = \varepsilon_r \varepsilon_0 A/d$, where C is the measured capacitance, ε_0 is the permittivity of free space (8.854×10^{-12} F/m), A is the area of the electrode, and d is the thickness of the dielectric. Capacitors with finite area electrodes have, in practice, measured capacitances that are higher than those predicted by the infinite parallel plate case due to fringing electric fields. This added contribution to the capacitance was modeled as being proportional to the electrode circumference [26], which falls off as the ratio of the electrode lateral dimensions to the dielectric thickness approaches infinity. The effect of fringing fields on the dielectric constant extracted from capacitance measurements was considered negligible, since the ratio of the electrode lateral dimensions to the film thickness is 1000:1. It has been reported [26] that the fringing fields introduce a 2% error in dielectric constant determinations for capacitors with an electrode diameter to film thickness ratio of 134:1, which is nearly an order of magnitude smaller than the ratio used here. The relative permittivity of the $SiAlO_2N$ films was determined to be 7.5 ± 0.05 extracted from a sample set of six capacitors.

3.3. $SiAlO_2N$ elastic constants

The elastic constants, C_{11} and C_{44}, of isotropic $SiAlO_2N$ films were determined by measuring the propagation of SAWs on devices covered with $SiAlO_2N$ thin film overlayers. When SAWs propagate along an uncoated crystal surface, the wave is dispersionless and the phase and group velocities are therefore the same [14]. However, when SAWs travel on a substrate beneath the $SiAlO_2N$ overlayer, the waves are dispersive in nature [14]. The measured velocity is, in this case, the group velocity, $v_g = \partial\,\omega/\partial\,k$, and not simply the phase velocity, $v_p = \omega/k$, where ω is the angular frequency of the wave and k is the wave number. The SAW group velocity was determined by considering the differential group delay between devices with different delay path lengths. The group delay, τ_g, of each device was determined from the slope of the phase of the transmission signal: $\tau_g = -\,\partial\,\phi/\partial\,\omega$, where ϕ is the phase of S_{21}. In principle, only two devices with different delay path lengths are needed to determine the SAW velocity. If the IDTs are identical in both devices, the delay time difference measured between the two devices can be attributed entirely to the difference in the delay path length. Device fabrication variations may result in slight differences in the measured velocities. To determine group velocity, one plots group delay as a function of delay path length and fits a straight line to the data points. The group velocity is given by the reciprocal of the slope of this fit. Though two points are all that is needed to define a line, the confidence in the value of the slope is presumed to increase with the number of data points. In this work, four data points were available from measurements on devices with four different path lengths (Fig. 2).

The extraction of elastic constants for $SiAlO_2N$ films was accomplished using a numerical implementation of the matrix method reported in reference [16]. This method can be used to calculate the SAW propagation characteristics of an n-layered structure provided the density as well as the elastic and dielectric properties of each layer are known [16]. Conversely, if the properties of film overlayers are at first unknown, the group velocity of multilayered structures can be measured and the acoustic properties of the layers can be extracted from these measurements [19].

Since the $SiAlO_2N$ film density, ρ, and permittivity, ε_r, were determined independently in this work, the remaining material properties required for acoustic wave calculations are film elastic constants. In the theory of linear elasticity, there are two independent elastic constants, C_{11} and C_{44}, for an isotropic homogenous medium such as the $SiAlO_2N$ film considered in this work [27]. The matrix method for SAWs [16] can be used to extract these constants using the SAW group velocity. Because C_{11} and C_{44} are both unknown for a general SAW orientation, any single orientation for which the SAW group velocity is measured will only provide a conditional relationship between the two elastic constants. To determine both C_{11} and C_{44}, SAW devices along two orientations that depend to different extents on each of the constants must be measured [19]. An open circuited boundary value problem is formulated based on the film thickness, ε_r [26] and density as well as the known constants of the quartz substrate [24], the measured v_g, and initial guesses for C_{11} and C_{44}. As discussed in [20], values of C_{11} and C_{44} are varied to minimize the difference between the calculated and measured v_g. The SAW v_g from a single orientation results in a curve of possible C_{11} vs. C_{44} values. From the v_g of a second orientation, a separate curve of possible C_{11} vs. C_{44} values is generated. The point where the two generated curves intersect determines the extracted value of $C_{11}$and C_{44}. For both quartz orientations and for all $SiAlO_2N$ film thicknesses used in this work, possible C_{11} values were plotted against their corresponding C_{44} values (Fig. 4). The targeted C_{11} and C_{44} values for $SiAlO_2N$ were selected by identifying regions where the curves for different crystal orientations intersected, assuming that the values of C_{11} and C_{44} did not vary with layer thickness.

The room temperature group velocities extracted for the quartz ST-X and ST-40° orientations with 20 nm, 200 nm, and 800 nm $SiAlO_2N$ overlayers are shown in Table 2. In general, the SAW velocities from both the ST-X and the ST-40° devices covered by a $SiAlO_2N$ overlayer are greater than on bare SAW devices, with the increase being more pronounced for thicker films. For the ST-X devices with an 800 nm $SiAlO_2N$ overlayer as well as the ST-40° devices with 20 nm and 200 nm $SiAlO_2N$ overlayers, the response of the four devices showed experimental differences credited to variations in device fabrication. For this reason, the group velocity was determined

Table 1
Measured capacitances and dielectric constants of $SiAlO_2N$ capacitors.

Capacitor #	C[a] (pF)	A (m^2*10^{-7})	ε_R
1	57.9	8.53	7.7 ± 0.2
2	43.9	6.60	7.3 ± 0.5
3	61.9	9.51	7.3 ± 0.2
4	44.9	6.89	7.4 ± 0.5
5	59.6	9.07	7.4 ± 0.2
6	–[b]	–	–
7	59.2	8.96	7.4 ± 0.2
8	48.5	–[c]	–

[a] Capacitances measured at 10 kHz.
[b] Short-circuited.
[c] Electrode was irregularly shaped and area could not be quantified.

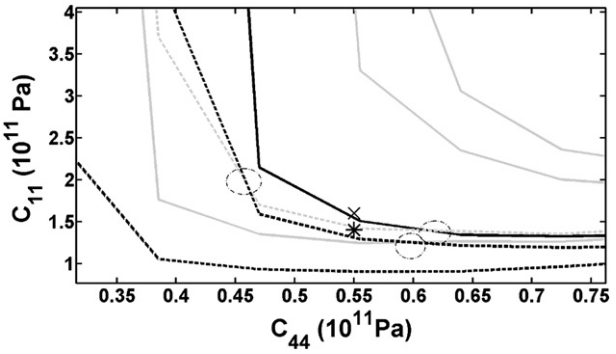

Fig. 4. C_{11} and C_{44} possibilities for quartz devices with 200 nm and 800 nm $SiAlO_2N$ overlayers. The gray and black traces denote the ST-X and ST-40° orientations, respectively. The solid lines represent devices with an 800 nm $SiAlO_2N$ overlayer while the dashed lines denote 200 nm $SiAlO_2N$ overlayers. The circles mark potential solutions for C_{11} and C_{44}. The 'X' marks the average of the three C_{11} and C_{44} potential solutions while the asterisk marks the C_{11} and C_{44} values reported in [20].

based on considering different sets of three out of the four devices. For these sets of devices, the different possible group velocities (extracted from different subsets of devices) are all listed in Table 2. It can be seen from the table that the agreement for the possible ST-40° velocities is better than 10 m/s (~0.3%), while the agreement for the ST-X devices with an 800 nm overlayer is slightly worse with the three possible velocities having a standard deviation from the mean of ~30 m/s (0.9%).

Using the extracted group velocities of SAW devices covered with the $SiAlO_2N$ overlayer and the measured density, thickness, and permittivity of the $SiAlO_2N$ films, possible combinations of C_{11} and C_{44} were plotted for each set of devices (Fig. 4). For sets of devices that gave ambiguous results for the group velocity, C_{11} and C_{44} combinations were calculated for each possible group velocity. For example, the three solid gray traces in Fig. 4 correspond to the three different group velocities given in Table 2 for the ST-X devices with an 800 nm $SiAlO_2N$ overlayer. The $C_{ii,}$ values determined using this method are very sensitive to the input group velocity. Varying the other film input parameters (ρ, ε_r, and thickness) by as much as 10% did not lead to as much variation in possible C_{ii} as did the uncertainty in group velocity. The results from devices with 20 nm $SiAlO_2N$ overlayers are not shown in Fig. 4 because they yielded the unreasonable result of $C_{11} \leq C_{44}$, which is not consistent with C_{11} being nearly three times larger than C_{44} for bulk SiAlON [20]. Because 20 nm is only a few tens of atomic layers, the elastic properties of these films may be more significantly altered by stresses at the film-substrate interface. For films with thickness between 200 and 800 nm, interfacial stresses do not appear to significantly affect the film elastic properties. While the interfacial stresses may increase with film thickness, the volumetric percentage of the thicker films that is affected by this boundary decreases. As the films increase in thickness, one might expect the determined C_{11} & C_{44} values to converge as the small portion of the film at the interface becomes less significant to the overall properties of the film. The three circles in Fig. 4 mark regions where the possible values of C_{11} and C_{44} are equal for different films, indicating potential solutions. These three C_{11} and C_{44} solutions were averaged together and their standard errors determined as a measure of the uncertainty in these values. The determined values, $C_{11} = 160 \pm 30$ GPa and $C_{44} = 55 \pm 5$ GPa, are indicated by an 'x' in Fig. 4. These results are consistent with the values of $C_{11} \approx 140$ GPa and $C_{44} \approx 55$ GPa (marked with an asterisk in Fig. 4) reported for bulk SiAlON materials doped slightly with yttrium [20]. It is noted that this comparison should be taken cautiously since many physical properties of thin films are different from their bulk counterpart, particularly when the latter has been doped. However, previously reported SiAlON elastic properties for comparison are very limited and this value is provided as a rough indication of what one might expect for elastic constants.

Table 2
Measured group velocity of quartz SAW devices with $SiAlO_2N$ coatings.

Orientation	$SiAlO_2N$ Thickness	V_g (m/s)
ST-X	Bare	3156.0
ST-X	20 nm	3153.1
ST-X	200 nm	3178.1
ST-X	800 nm	3243.8
		3252.0
		3198.7
ST-40°	bare	3270.6
ST-40°	20 nm	3279.9
		3271.8
ST-40°	200 nm	3278.4
		3271.3
ST-40°	800 nm	3294.1

3.4. Influence of $SiAlO_2N$ overlayers on SAW temperature coefficient of delay (TCD)

The measured TCDs for quartz ST-40° SAW device orientations with 20 nm, 200 nm, and 800 nm $SiAlO_2N$ overlayers are compared with the bare device TCDs in Fig. 5. The TCD appears to be insensitive to the presence of the overlayer up to 200 nm film thickness. A similar effect was observed for the quartz ST-X orientation. For both orientations, the devices with 20 nm and 200 nm $SiAlO_2N$ overlayers have the same TCD as a bare device, within the estimated ~10 ppm/°C uncertainty of the measurements. However, the TCD of both orientations with a 800 nm $SiAlO_2N$ overlayer has a large room temperature offset and goes through a pronounced maximum between 80 °C and 100 °C. For the ST-40° SAW device with an 800 nm $SiAlO_2N$ coating, the room temperature TCD is increased by ~20 ppm/°C, giving these devices a TCD of zero for temperatures between 20 °C and 40 °C. The pronounced maximum in the TCD as a function of temperature is more striking for the ST-X orientation, where the room temperature TCD offset is nearly 50 ppm/°C. Furthermore, the maximum difference between the 800 nm coated ST-X devices and the bare device is greater than 200 ppm/°C compared to the maximum difference of 90 ppm/°C for the ST-40° devices.

The matrix method of [16] calculates SAW propagation characteristics by matching dynamic displacements and stresses at interfacial boundaries, but it does not consider static interfacial stresses that may be generated at the film/substrate interface. These stresses can be significant, particularly at elevated temperatures if the film and substrate thermal coefficients of expansion (TCEs) are not well matched. For the quartz orientations measured in this work, the TCE

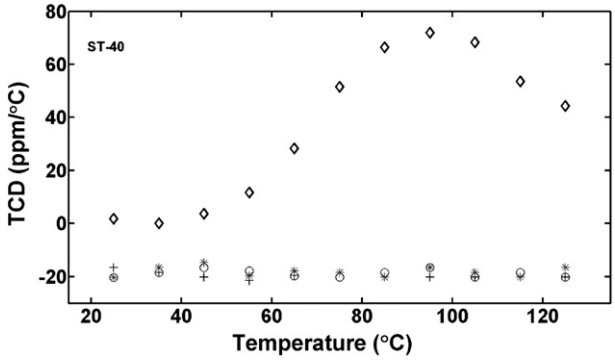

Fig. 5. TCD of quartz ST-40° devices with varying thicknesses of $SiAlO_2N$ overlayers. Symbols correspond to the following thickness of $SiAlO_2N$ coatings: + = bare, O = 20 nm, ⋆ = 200 nm, ◊ = 800 nm.

along the SAW propagation direction is roughly 13 ppm/°C, while that of $SiAlO_2N$ is significantly lower at 3.6 ppm/°C (bulk value) [28]. For films with a thickness of 3% of the SAW wavelength, such as those used in this work, the TCE of the film may play an important role in determining the device TCD.

The room temperature operating frequencies, f_0, and transmission losses, $|S_{21}|_{max}$, of the six measured LGT devices are shown in Table 3. The $SiAlO_2N$ coated devices exhibit a shift in the operating frequencies on the order of hundreds of kilohertz when compared to bare devices. This frequency shift, which is greater than the ≤10 kHz uncertainty in the measurement, may result from small differences in device fabrication, from the presence of the $SiAlO_2N$ film, or both. The transmission losses in Table 3 are slightly greater on average for the coated compared to the bare devices. When the slowest bulk acoustic wave (BAW) mode in $SiAlO_2N$ is greater than the slowest BAW in the LGT substrate, energy scattering is favored away from the surface and into the bulk of the substrate [29]. The relevant BAW velocities in LGT, $SiAlO_2N$, and quartz were calculated using the Christoffel equation [27] to investigate if the film induced energy scattering away from the surface. For $SiAlO_2N$, the shear BAW has a phase velocity of 4432 m/s, which is faster than the slowest LGT BAW along all of the orientations for which SAW devices were fabricated. The fact that the BAW velocities in the film are faster than those of the LGT substrate may explain the increased transmission loss in the $SiAlO_2N$ coated devices with respect to the bare devices. The increase in transmission loss for the LGT devices is around a few dB in most cases and 8.5 dB in the worst case for the (90°, 23°, 123°) device. Considering that the noise floor in the $|S_{21}|$ measurements is in the −60 to −90 dB range, all devices were still easily measured despite the small increase in transmission loss.

Table 3 shows the measured TCD for the six LGT delay lines with both bare and $SiAlO_2N$ coated delay paths. The room temperature TCDs of the coated devices and the bare devices are the same within the measurement uncertainty, unlike the case with the quartz based devices. The very similar temperature behavior of the coated devices to the bare devices persists over the entire temperature range measured, as can be seen in Fig. 6, which shows the $\Delta f/f_0$ ($\Delta f = f - f_0$, where f is the operating frequency at a given temperature) and TCD for a (90°, 23°, 119°) LGT SAW device plotted against temperature; this data is representative of all six LGT SAW orientations measured. The 800 nm thick $SiAlO_2N$ film serves to reduce the TCD of the (90°, 23°, 119°) device by 1–2 ppm/°C over the entire temperature range and shifts the bare device turnover temperature of 58 °C up to 62 °C. The (90°, 23°, 123°) LGT orientation also exhibits an inherently low SAW TCD [4] and the turnover temperature of a device along this orientation with a 500 nm $SiAlO_2N$ overlayer was shifted from the bare device value of 47 °C up to 54 °C. A notable property of the LGT TCD vs. temperature behavior is the absence of a pronounced maximum in TCD as was observed with the quartz devices. With respect to the insensitivity of the LGT TCD to $SiAlO_2N$ films as thick as 800 nm, it is interesting to note that the TCE for the LGT orientations measured is only about 6 ppm/°C which is better matched to the 3.6 ppm/°C TCE of bulk SiAlON [28].

Table 3
Measured LGT SAW properties with 500 nm and 800 nm $SiAlO_2N$ overlays.

Ψ (°)	$SiAlO_2N$ Thickness (nm)	f_0 (MHz)	$\|S_{21}\|_{max}$ (dB)	TCD (ppm/°C)
0	0	76.363	−18.2	−50.3
	500	76.808	−19.3	−48.9
13	0	72.910	−26.7	−70.8
	800	75.538	−26.1	−70.6
48	0	72.218	−22.2	−68.7
	500	72.398	−24.3	−70.0
77	0	72.706	−29.5	−75.6
	800	73.057	−34.9	−72.9
119	0	85.398	−17.2	−11.5
	800	86.180	−21.4	−7.3
123	0	85.985	−28.8	−6.0
	500	86.378	−37.3	−4.4

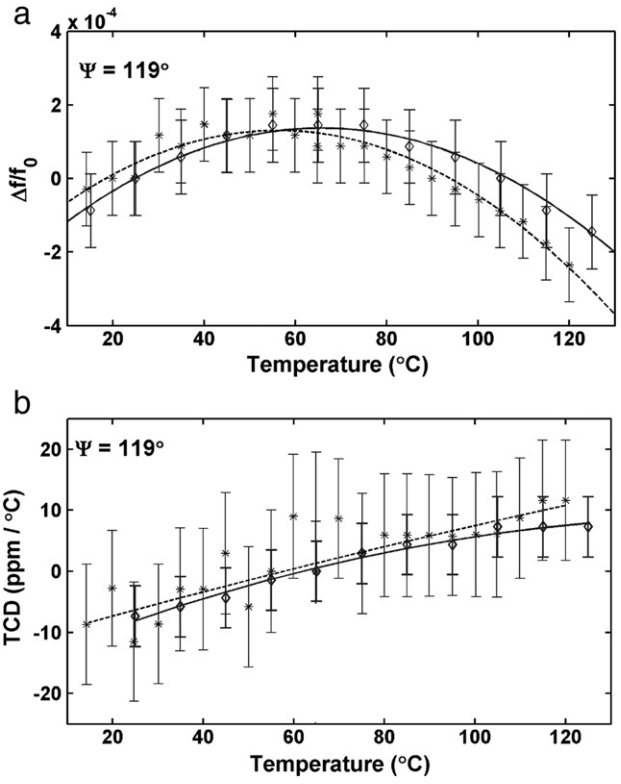

Fig. 6. (a) $\Delta f/f_0$ and (b) TCD for LGT (90°, 23°, 119°) with 800 nm thick $SiAlO_2N$ overlayer. Asterisks are experimental data points with no $SiAlO_2N$ and the diamonds are experimental data points with an 800 nm thick $SiAlO_2N$ overlayer. The dashed and solid lines show best fit curves to the bare device and $SiAlO_2N$ coated device data, respectively.

4. Conclusions

The properties of SAW devices coated with $SiAlO_2N$ overlayers have been investigated using devices fabricated on both quartz and langatate piezoelectric substrates. $SiAlO_2N$ films deposited by RF magnetron co-sputtering were reproducibly deposited onto the SAW devices, and the chemical composition, density, thickness, and dielectric permittivity of $SiAlO_2N$ films were determined. Parallel plate capacitors with 1 mm lateral dimensions were fabricated for a 1 μm thick $SiAlO_2N$ dielectric layer between Al electrodes, and the capacitance measurements yielded a value for the $SiAlO_2N$ relative permittivity of $\varepsilon_r = 7.5 \pm 0.05$. $SiAlO_2N$ elastic constants C_{11} and C_{44} were extracted using a numerical implementation of the matrix method for SAWs traveling in multilayer structures and they were found to be $C_{44} = 55 \pm 5$ GPa and $C_{11} = 160 \pm 30$ GPa.

Empirical observations of the effect of $SiAlO_2N$ coatings on quartz and LGT SAW delay line TCDs were also reported. Quartz SAW device operating frequencies were only slightly perturbed by the presence of $SiAlO_2N$ films as thick as 800 nm. Although the TCDs of quartz devices with 20 nm and 200 nm $SiAlO_2N$ coatings were unaffected by the presence of the $SiAlO_2N$ film, devices with 800 nm thick overlayers exhibited room temperature TCDs up to almost 50 ppm/°C larger than the bare devices. Further, the quartz devices with the thickest $SiAlO_2N$ coatings showed large and pronounced maxima in TCD near 100 °C for both the ST-X and ST-40° orientations. For the ST-X cut in particular, the TCD was nearly 250 ppm/°C larger at 100 °C than that of the bare device. The operating frequency of LGT SAW devices was more affected by the presence of a $SiAlO_2N$ overlayer

compared to quartz devices. Additionally, even with transmission losses up to 8.5 dB more for the 500 nm $SiAlO_2N$ coated LGT (90°, 23°, 123°) compared to the bare device of the same orientation, the transmission signal was still easily measurable. Unlike the quartz devices, the TCDs of the LGT devices were minimally affected by the presence of $SiAlO_2N$ coatings up to 800 nm thick. This result might be attributed to the fact that the temperature coefficient of expansion for the LGT orientations (~6 ppm/°C) is more closely matched to the 3 ppm/°C TCE for $SiAlO_2N$ compared to the TCE of ~13 ppm/°C for quartz ST-X and ST-40° orientations.

The result that the TCD of LGT SAW devices is hardly perturbed by the presence of a 800 nm thick $SiAlO_2N$ overlayer is very important, particularly in the context of high temperature SAW sensor devices operating in harsh mechanical and/or chemical environments. The results of this work suggest that LGT-based devices requiring zero TCD can be designed by considering only the bare substrate and not a multi-layer structure, which greatly simplifies device design and modeling in this temperature range.

Acknowledgments

This work was supported by the Air Force Office of Scientific Research (AFOSR) grant # FA9550-07-1-0519 (SAW device fabrication and characterization) and the National Science Foundation (NSF) grant # 0840045 (SiAlON film development).

References

[1] J.A. Kosinski, Int. J. High Speed Electron Syst. 10 (4) (2000).
[2] H. Thanner, P.W. Krempl, W. Wallnofer, P.M. Worsch, Vacuum 67 (3–4) (2002) 687.
[3] M.N. Hamidon, V. Skarda, N.M. White, F. Krispel, P. Krempl, M. Binhack, W. Buff, Sens. Actuators, A Phys. 123–24 (2005) 403.
[4] B.T. Sturtevant, M.P. da Cunha, IEEE Trans. Ultrason. Ferroelectr. Freq. Control 57 (3) (2010) 533.
[5] J. Haines, O. Cambon, D.A. Keen, M.G. Tucker, M.T. Dove, Appl. Phys. Lett. 81 (16) (2002) 2968.
[6] K.H. Jack, J. Mater. Sci. 11 (6) (1976) 1135.
[7] M. Mitomo, Y. Tajima, J. Ceram. Soc. Jpn. 99 (10) (1991) 1014.
[8] J.I. Krassikoff, G.P. Bernhardt, M. Call, T.A. Dunn, D.D. More, R.J. Lad, 46th Annual Society of Vacuum Coaters Technical Conference, 2003, p. 627.
[9] B. Bitterlich, S. Bitsch, K. Friederich, J. Eur. Ceram. Soc. 28 (5) (2008) 989.
[10] Y. Nakamura, M.K. Kurosawa, T. Shigematsu, K. Asai, IEEE Ultrason. Symp. Proc. 1 and 2 (2003) 1766.
[11] M. Pereira da Cunha, T. Moonlight, R. Lad, G. Bernhardt, D.J. Frankel, IEEE Ultrason. Symp. Proc. 1–6 (2007) 2107.
[12] D.J. Frankel, G.P. Bernhardt, B.T. Sturtevant, T. Moonlight, M. Pereira da Cunha, R.J. Lad, IEEE Sens. (2008) 82.
[13] T.E. Parker, M.B. Schulz, IEEE Trans. Sonics Ultrason. Su22 (3) (1975) 227.
[14] T.E. Parker, H. Wichansky, J. Appl. Phys. 50 (3) (1979) 1360.
[15] M.F. Lewis, IEEE Trans. Sonics Ultrason. 27 (3) (1980) 143.
[16] E.L. Adler, IEEE Trans. Ultrason. Ferroelectr. Freq. Control 37 (6) (1990) 485.
[17] D.P. Morgan, Surface-Wave Devices for Signal Processing, Elsevier, 1991.
[18] N. Dewan, M. Tomar, K. Sreenivas, V. Gupta, IEEE Int. Ultrason. Symp. Proc. 1–4 (2005) 1311.
[19] D. Gallimore, T. Moonlight, M.P. da Cunha, IEEE Int. Ultrason. Symp. Proc. (2009) 2797.
[20] H. Lemercier, T. Rouxel, D. Fargeot, J.L. Besson, B. Piriou, J. Non-Cryst. Solids 201 (1–2) (1996) 128.
[21] S.C. Moulzolf, D.J. Frankel, R.J. Lad, Rev. Sci. Instrum. 73 (6) (2002) 2325.
[22] D.A. Shirley, Phys. Rev. B 5 (12) (1972) 4709.
[23] J.F. Moulder, J. Chastain, Handbook of X-Ray Photoelectron Spectroscopy: A Reference Book of Standard Spectra for Identification and Interpretation of XPS Data, Physical Electronics Division, Perkin-Elmer Corporation, 1992.
[24] B.J. James, Proc 42nd Annual Freq Contr Symp 1988 (IEEE Cat. No.88CH2588-2), 1988, p. 146.
[25] U. Pietsch, V. Holý, T. Baumbach, High-resolution X-ray Scattering from Thin Films to Lateral Nanostructures, Springer-Verlag, 2004.
[26] V.E. Bottom, J. Appl. Phys. 43 (4) (1972) 1493.
[27] B.A. Auld, in: R.E. Krieger (Ed.), Acoustic Fields and Waves in Solids, 1990.
[28] M. Fukuhara, I. Yamauchi, J. Mater. Sci. 28 (17) (1993) 4681.
[29] D. Royer, E. Dieulesaint, D.P. Morgan, Elastic Waves in Solids I: Free and Guided Propagation, Springer, 2000.